Energy & Environmental Science

ROYAL SOCIETY OF CHEMISTRY

PAPER

View Article Online
View Journal | View Issue

Cite this: *Energy Environ. Sci.*, 2026, **19**, 849

Unveiling the mechanism of lithium-mediated nitrogen reduction *via operando* X-ray scattering in a flow cell with hydrogen oxidation

Niklas H. Deissler, [a] J. Bjarke V. Mygind, [a] Valerie A. Niemann, [bc] Jakob B. Pedersen, [a] Valentin Vinci, [d] Shaofeng Li, [a] Xianbiao Fu, [a] Thomas F. Jaramillo, [bc] Jakob Kibsgaard, [a] Jakub Drnec [d] and Ib Chorkendorff *[a]

Received 30th October 2025,
Accepted 16th January 2026

DOI: 10.1039/d5ee06529a

rsc.li/ees

The lithium-mediated nitrogen reduction reaction (Li-NRR) is currently the most promising strategy for electrochemical ammonia synthesis. In this study, we present an *operando* grazing incidence wide angle X-ray scattering (GI WAXS) investigation using an improved electrochemical flow cell that enables hydrogen oxidation at the anode and thereby eliminates the need of a sacrificial proton donor. The improved cell design also increases nitrogen availability and mass transport, achieving ammonia faradaic efficiencies (FEs) up to 36%. This setup allows direct analysis of reaction intermediates and the solid electrolyte interphase (SEI) using state-of-the-art diglyme-based electrolytes. We identify lithium amide ($LiNH_2$) as the only stable, crystalline intermediate, providing direct insight into the Li-NRR mechanism. Notably, in diglyme-based electrolytes, the SEI composition differs significantly from that in tetrahydrofuran-based systems, with reduced LiF content and the formation of previously unreported crystalline diglyme–lithium salt complexes. These species likely influence ammonia selectivity and long-term stability. Our findings highlight how the electrolyte composition and cell architecture govern Li-NRR selectivity and efficiency, offering a foundation for the rational design of next-generation SEI layers and solid electrolytes to enable scalable electrochemical ammonia synthesis.

Broader context

Ammonia is one of the world's most produced chemicals, with over 180 million tons produced annually, mainly for synthetic fertilizers. The lithium-mediated nitrogen reduction reaction (Li-NRR) has emerged as a promising, sustainable alternative to the energy-intensive Haber–Bosch process, operating at ambient temperature and pressure. In the Li-NRR, lithium metal is electrodeposited from an organic electrolyte. Nitrogen then reacts with the lithium, forming intermediate lithium–nitrogen species that are then protonated to yield ammonia. However, lithium also reacts with the electrolyte, creating the solid electrolyte interphase (SEI) layer. Both the precise reaction mechanism and the role of the SEI layer however remain unclear. Previous *operando* studies have provided valuable insights, but experimental limitations meant these investigations were conducted under conditions that differed significantly from those used in advanced, state-of-the-art systems. In this work, we employ *operando* grazing incidence wide-angle X-ray scattering (GI WAXS) within an optimized experimental setup, providing insights in both the reaction mechanism and the composition of the SEI layer under high-performance conditions.

Introduction

Ammonia is one of the most produced chemicals in the world, mainly for its use in fertilizer production.[1,2] It has also been proposed as a potential energy carrier in the future.[3] Currently ammonia is almost exclusively produced in the Haber–Bosch process which requires high pressures and temperatures and is therefore only viable in large scale facilities.[4] An electrochemical process at ambient conditions would allow for decentralized ammonia production at the point of use and is more compatible with the intermittency of renewable energy production. The lithium-mediated nitrogen reduction reaction (Li-NRR) is currently the most promising strategy for electrochemical ammonia production.[5–9] In the Li-NRR, lithium, plated electrochemically from an organic electrolyte, reacts with nitrogen to

[a] *Department of Physics, Technical University of Denmark, Kongens Lyngby, Denmark, icho@dtu.dk*
[b] *Department of Chemical Engineering, Stanford University, Stanford, CA, USA*
[c] *SUNCAT Center for Interface Science and Catalysis, SLAC National Accelerator Laboratory, Menlo Park, CA, USA*
[d] *Experiments Division, European Synchrotron Radiation Facility, Grenoble, France*

form Li–N intermediates which are protonated by a proton donor/shuttle to form ammonia. However, lithium can also directly react with protons forming hydrogen. Therefore, limiting this competing reaction is essential to achieving high selectivity towards ammonia.[10] Decomposition of the electrolyte also leads to the formation of the solid electrolyte interphase (SEI) layer, comparable to that formed in Li-batteries. By regulating mass transport processes to the plated lithium, the SEI layer plays a critical role in limiting undesired side reactions, including hydrogen evolution and further electrolyte decomposition. There have been substantial efforts to determine and understand electrode processes in the Li-NRR by using *in situ* and *operando* techniques such as grazing incidence wide angle X-ray scattering (GI WAXS) and neutron reflectometry.[11–13] While valuable insights were gained in these studies, all of them employed batch cells with faradaic efficiencies (FEs) towards ammonia below 3%. Furthermore, these batch cells rely on sacrificial agents as proton source as well as anodic electrolyte decomposition as counter electrode reaction. Recent studies in the field of Li-NRR not only showed FEs of almost 100%[14,15] but also the development of a flow cell system that includes the hydrogen oxidation reaction (HOR) on the anode, allowing for continuous ammonia production without requiring a sacrificial agent.[16] This system was also used to develop a diglyme based electrolyte allowing for long term operation up to 300 h with an FE of 64% at a current density of -6 mA cm^{-2}.[17] As the experimental conditions in previously used *operando* batch cells are not comparable to those in current state-of-the-art Li-NRR systems, better performing electrochemical cells are necessary for *in situ* and *operando* studies.[18] Here we present an *operando* study using a new electrochemical cell allowing for electrolyte flow, HOR on the anode and FEs up to 36%.[19] This cell was used to study the Li-NRR reaction mechanism and the beneficial properties of diglyme based electrolytes under reaction conditions comparable to state-of-the-art flow cell systems allowing for high performance ammonia synthesis.

Valuable insights into the Li-NRR reaction mechanism were gained as $LiNH_2$ was identified as the only stable (crystalline) intermediate. The beneficial properties of diglyme based electrolytes were studied and unlike in tetrahydrofuran (THF) based electrolytes, LiF was not the predominant SEI species. Instead, diglyme complexes formed, especially when pulsed deposition was used.

Experimental

Synchrotron experiments were performed at the ID31 beamline at the European Synchrotron Radiation Facility (ESRF). The experimental setup is schematically shown in Fig. 1A and a photograph is shown in Fig. S1. For all experiments, a previously described 3D-printed PEEK cell was used.[19] The cells were assembled in an argon filled glovebox. Cu(111) single-crystal working electrodes were Ar-sputtered and annealed in vacuum or annealed in a 1 : 3 H_2 : Ar atmosphere, and then transferred to the glove box without air exposure. A previously described stainless steel mesh gas diffusion electrode (GDE) with electro plated PtAu catalyst was used as counter electrodes.[16] A Pt wire was used as a pseudo-reference electrode. If not otherwise mentioned, electrolytes consisted of 1 M electrolyte salt ($LiBF_4$, LiTFSI, or LiFOB) and 0.125 vol% EtOH dissolved in diglyme. In one experiment (denoted as $LiBF_4$ + H_2O) 0.125 vol% H_2O was also added to the electrolyte. The high-energy monochromatic synchrotron X-ray beam (E = 75 keV) was focused on the single crystal working electrode at an incidence angle of 0.05° to perform GI WAXS measurements. Near atomically flat single crystal electrodes in combination with a small incidence angle close to the critical angle result in the formation of a surface confined evanescent wave significantly increasing the surface sensitivity, which allows for the detection of small amounts of deposits on the electrode.[20] 2D detector images were recorded by means of a Dectris Pilatus CdTe 2M detector positioned 1.3 m behind the sample, allowing for a q-range of ~0.4–10 Å^{-1}. The absolute value of the scattering vector $\vec{q}$ is defined as $q = |\vec{q}| = \frac{4\pi}{\lambda}\sin\left(\frac{2\theta}{2}\right)$ with the wavelength λ and the angle between incident and scattered beam 2θ. Radial integration of 2D detector images yields 1D diffractograms. During the experiment the electrolyte was continuously saturated with N_2 and pumped through the cell. The counter electrode was continuously supplied with H_2 through a flow field. After an initial open circuit voltage (OCV) period (>30 min) a linear sweep voltammetry (20 mV s^{-1}) was conducted until the current increased to >4 mA cm^{-2}, indicating the onset of Li plating. Then the deposition technique used throughout the rest of the experiment was initiated. If not otherwise stated a current density of -4 mA cm^{-2} was applied using either a constant current (Chrono Potentiometry; CP) or pulsed deposition technique. Pulsed deposition consisted of 1 min deposition with a current of -4 mA cm^{-2}, followed by an OCV resting period until the working electrode increased to a potential >-2.5 V *vs.* Pt.[17] Constant current and pulsed deposition experiments with $LiBF_4$ were conducted twice. If not otherwise mentioned, the same qualitative trends were observed in both experiments. Ammonia content was measured in the electrolyte and the gas outlet acid traps. After the experiment the working electrode was submerged in water and ammonia content was determined in the resulting solution. Further experimental details, electrochemical data (Fig. S2–S5), overview diffractograms and overview diffractograms at OCV (Fig. S6–S13) can be found in SI.

Results and discussion

As shown in Fig. 1B, faradaic efficiencies exceeding 30% were achieved with the new cell and setup, which were substantially higher than those reported in previous *operando* and *in situ* studies.[11–13] While differences in SEI formation might also play a role these high FEs can be primarily attributed to improved N_2 transport. The observed FEs correspond to the conversion of 6 times more N_2 to ammonia than what is present in the electrolyte chamber of the cell at any given time, which is not

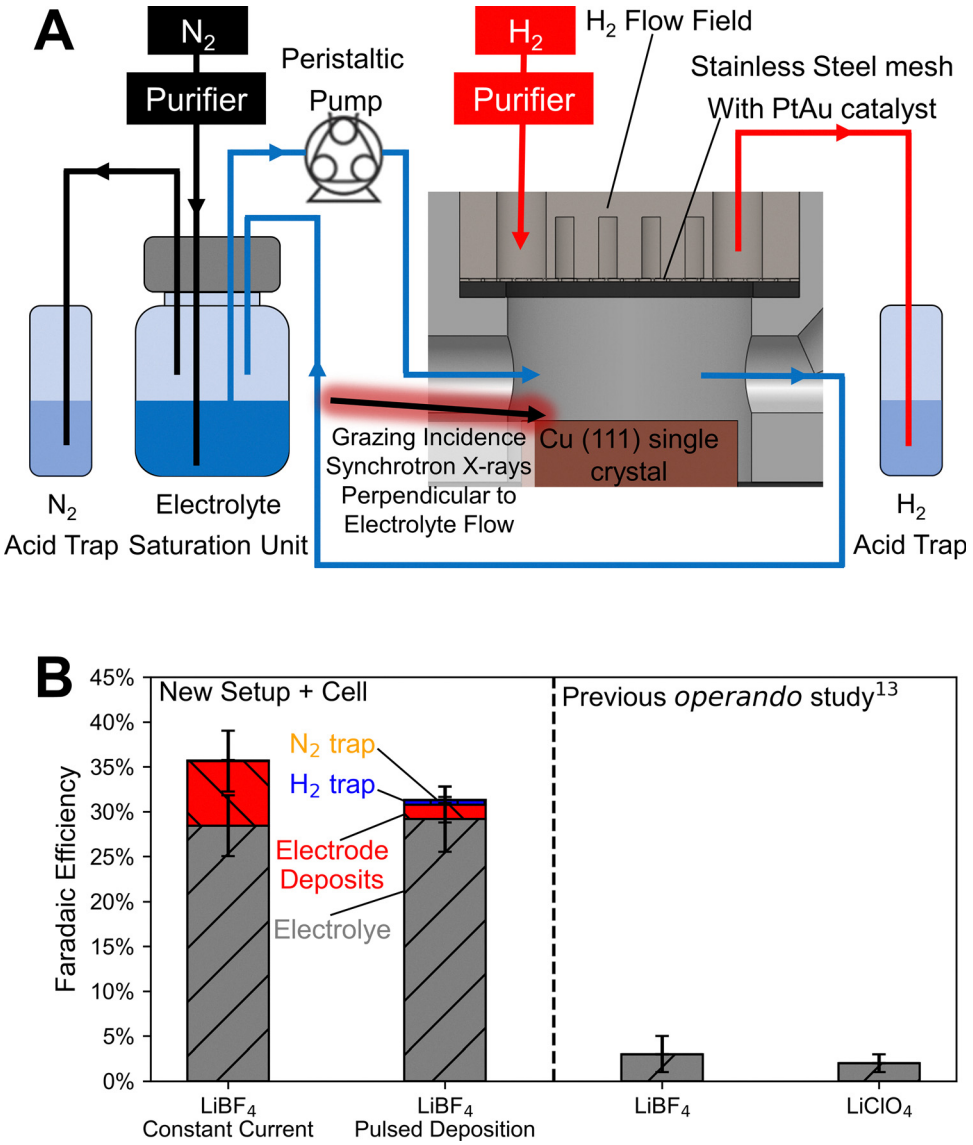

Fig. 1 (A) Schematic depiction of the experimental setup. (B) Ammonia FE comparison between this study, using a new setup and cell and a previous *operando* study.[13] Error bars indicate standard deviation from at least three independent experiments of which two were performed at the synchrotron. In constant current experiments a current of -4 mA cm^{-2} was applied until 7.5C was passed. In pulsed deposition experiments a current of -4 mA cm^{-2} was applied for 1 min, followed by a resting period at OCV until the working electrode potential had increased to > -2.5 V *vs.* Pt. A Cu(111) single crystal was used as the working electrode and a Pt wire as reference electrode. A stainless-steel mesh with electrodeposited PtAu catalyst, supplied with H_2 was used as counter electrode. Electrolytes consisted of 1 M $LiBF_4$ dissolved in diglyme and 0.125 vol% EtOH.

possible in batch cells without electrolyte flow.[19,21] Continuous saturation of the electrolyte, in combination with convection due to the electrolyte flow, replenished consumed N_2 at the working electrode. Notably in batch cells, diglyme-based electrolytes have been shown to perform worse than-THF based electrolytes, highlighting the necessity of enabling HOR on the anode.[22,23]

As shown in Fig. 1B, no improvement in FE was observed with pulsed deposition in the setup used. It is important to note that the ethanol concentration was optimized for constant current conditions and was not changed for pulsed deposition experiments, potentially resulting in a non-optimal concentration for the latter. The beneficial effect of reduced Li accumulation with pulsed deposition will be more pronounced the more charge is passed. In the presented experiments relatively small amounts of charge were passed in each experiment (5C or 7.5C). Furthermore, in each experiment after Li deposition, OCV was measured for at least 30 min before the electrolyte was removed from the cell. During this time, accumulated Li continued to react with N_2, as highlighted by the higher amounts of ammonia detected in the electrode deposits in constant current experiments. Uninterrupted Li deposition in constant current experiments likely lead to the accumulation of more deposits on the electrode, causing more ammonia to be trapped in these deposits. In previously reported long-term flow cell experiments the majority of ammonia was detected in the

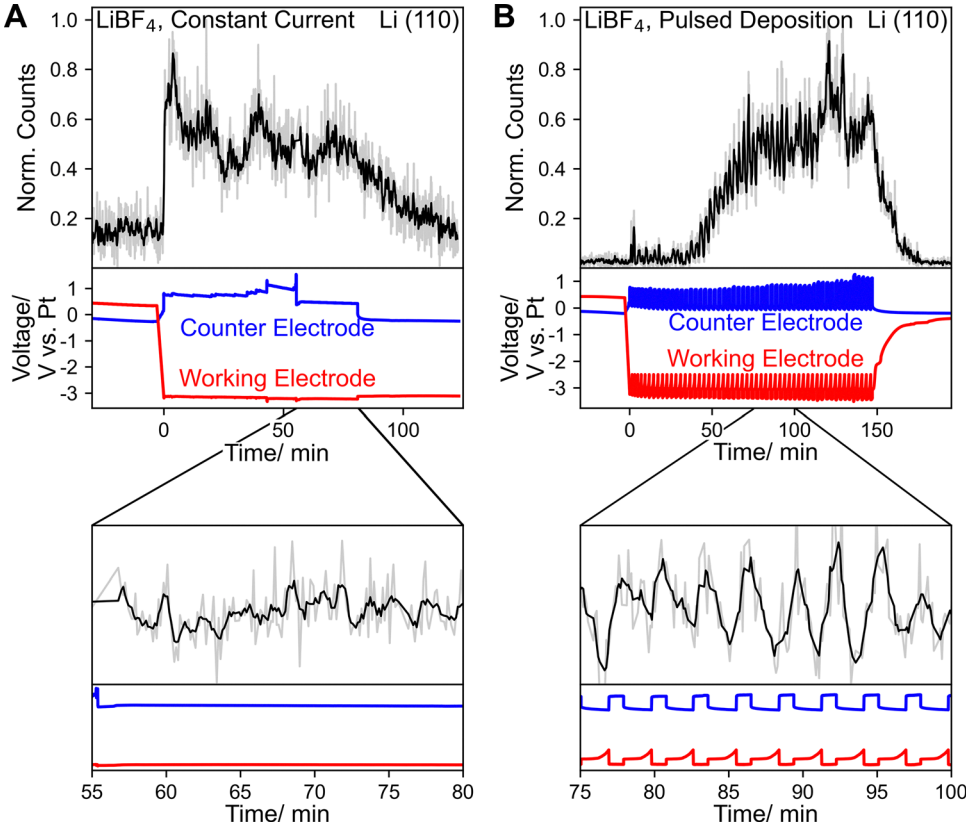

Fig. 2 Time traces of the intensity of the Li(110) diffraction peak when constant current (A) or pulsed deposition (B) was used. A linear background was subtracted from the integrated WAXS pattern, prior to determining peak maxima for the time traces. In constant current experiments a current of −4 mA cm^{-2} was applied until 7.5C was passed. In pulsed deposition experiments 54 cycles (corresponding to 5C) consisting of applying a current of −4 mA cm^{-2} for 1 min, followed by a resting period at OCV until the working electrode potential had increased to >-2.5 V *vs.* Pt were conducted. A Cu(111) single crystal was used as the working electrode and a Pt wire as reference electrode. A stainless-steel mesh with electrodeposited PtAu catalyst, supplied with H_2 was used as counter electrode. Electrolytes consisted of 1 M $LiBF_4$ dissolved in diglyme and 0.125 vol% EtOH.

gas phase.[17] In contrast, very little ammonia was detected in the acid traps at the gas outlets, indicating that the electrolyte was not fully saturated with ammonia because less charge was passed compared to long-term experiments. Occasionally, ammonia was detected in the H_2 acid traps, however this was most likely caused by electrolyte cross over through GDE on the anode side. It should be noted that despite improved mass transport compared to previous *operando* batch cells, FEs are still significantly lower than in flow cells with gas diffusion electrodes.[16,17] This difference suggests that despite the improvements in N_2 mass transport the overall reaction might still be limited by N_2 availability, which explains that no improvement in FE was observed for pulsed deposition experiments.[16]

Fig. 2A shows the time trace of the Li(110) diffraction peak when constant current (−4 mA cm^{-2}) was used, whereas Fig. 2B shows the same when pulsed deposition (−4 mA cm^{-2}/OCV) was used. As shown in Fig. 2A the intensity of the Li (110) peak immediately increased when constant current was applied, showing Li plating. During the experiment, the intensity did not increase continuously, indicating that plated Li continued to react throughout the experiment. At OCV, the working electrode potential remained at −3.4 V *vs.* Pt for ∼30 min after the experiment, indicating significant accumulation of metallic Li on the electrode surface. This potential was also maintained when Li could no longer be clearly detected by GI WAXS, potentially suggesting the formation of amorphous Li deposits or very small coherently scattering domains. Pulsed deposition, often referred to as cycling, has previously been shown to increase ammonia FEs and stability.[24] As shown in Fig. 2B the overall Li(110) intensity oscillated, corresponding to the deposition pulses. An increase in intensity was observed during the deposition pulses, followed by a decrease during the rest period. This behavior is expected as at OCV, deposited Li reacts to either form SEI species or ammonia, leading to its dissolution or conversion into other species. However, after an initial period of approximately 35 min an overall increase in Li(110) intensity was observed, despite returning to a working electrode potential above −2.5 V *vs.* Pt after each deposition pulse. This observation suggests the formation of lithium electronically disconnected from the working electrode. In the context of Li-metal batteries electronically disconnected Li is often referred to as "dead lithium" since it does not participate in the electrochemical reaction anymore.[25,26] It should be noted that in the Li-NRR so called "dead lithium" can still be active towards making ammonia, as all steps following electrochemical Li plating can occur chemically.[27] Despite this, "dead lithium" formation is most

likely not desirable as it is likely accompanied by processes that jeopardize the integrity of the SEI layer, thereby mitigating any beneficial effect it may have. Continuous reformation of the SEI layer is also undesirable for long-term stability. It is likely that some "dead lithium" also formed during the constant current experiments. However, due to the continuous plating of Li in these experiments, this cannot be confirmed as it is not possible to distinguish between "dead Li" and electrically connected Li in these experiments. A broad peak, centered around 2.50 $Å^{-1}$, shown in Fig. S14 could correspond to the formation of an amorphous Li phase, but is more likely related to $LiNH_2$ formation. The peak could also correspond to the LiOH(101) reflection, however the more intense LiOH(110) peak was not observed (Fig. S15).

As shown in Fig. 2B, after the final deposition pulse the working electrode potential increased almost immediately, suggesting less Li accumulation compared to constant current deposition.[28] Improved performance when using pulsed deposition has previously been attributed to this decreased Li accumulation.[24] Like in our previous study, the intensity originating from Li was not distributed homogeneously over the corresponding detector pixels, implying contributions from only a limited number of crystallites (Fig. S16–S18).[13] However, Li signals were generally weaker under all experimental conditions. One contributing factor could be the higher current density, likely leading to less ordered Li deposition, a less crystalline Li phase and smaller Li crystallites. Nevertheless, even when using a lower current density of -2 mA cm^{-2}, Li intensities remained comparatively small (Fig. S14, S15 and S18). Therefore, the improved mass transport characteristics and/or differences in the SEI layer are likely responsible for a decrease in Li accumulation compared to our previous study. Especially, when constant current was used Li signals were less pronounced suggesting the formation of a more amorphous Li phase or smaller crystallites compared to pulsed deposition experiments. Likely the resting time between deposition pulses allows for a restructuring in favor of bigger crystallites before Li is consumed by reactions.

As shown in Fig. 2A and B, throughout the experiments, most of the time the counter electrode potentials remained below 1 V *vs.* Pt, indicative of HOR. Increases in counter electrode potentials were always accompanied by the accumulation of bubbles, close to the anode. When the bubbles left the cell either unassisted or by temporarily increasing the flow-rate, anode potentials immediately decreased. Bubbles were likely caused by both hydrogen formation at the cathode and gas crossover on the anode.

In Fig. 3A and B the time development of the $LiNH_2$(112) peaks for constant current and pulsed deposition, are shown. The corresponding diffraction peaks are shown in Fig. 3C. With constant current, the $LiNH_2$(112) peak was less pronounced, suggesting a lower degree of crystallinity or the formation of fewer deposits. In our previous work this peak was also observed but could not be assigned with certainty, due to its low intensity.[13] Consistent with higher FEs, here the $LiNH_2$(112) peak is clearly visible with higher intensity in all experiments. In the pulsed deposition experiment peaks at higher q-vectors also have high enough intensities to clearly distinguish between $LiNH_2$ and Li_2NH (Fig. S19), identifying $LiNH_2$ as the only crystalline $Li_xN_yH_z$ species observed. The accumulation of any reaction intermediate suggests that their protonation is limited either kinetically or possibly by the availability of protons. The continual apparent accumulation of only $LiNH_2$, could suggest that it is the most stable reaction intermediate and reaction steps following its formation are limited. It should be noted that the apparent absence of other reaction intermediates, such as Li_2NH, does not mean that they were not present. Rather, they might not have accumulated in sufficient (crystallite) quantities to be detected by GI WAXS, either because they were consumed during fast reaction steps or formed as non-crystalline phases. Fig. 3A and B show the time development of the $LiNH_2$(112) peaks for constant current and pulsed deposition. In both cases, an overall increase in intensity was observed, in parallel to the increase in Li(110) intensity. Similar to the Li(110) signal, the $LiNH_2$ signal also oscillates in response to the deposition pulses, however, as shown in Fig. 3D the signal is phase-shifted. A peak in Li(110) intensity during deposition, was followed by an increase in $LiNH_2$(112) intensity during the resting period when no current or potential was applied, corresponding to the conversion of Li to $LiNH_2$. This observation is noteworthy as it confirms that the conversion of Li to $LiNH_2$ can occur purely chemically and does not require an electrochemical step as naturally at OCV there is no current between the electrodes.[27] During the deposition pulses a decrease in $LiNH_2$(112) intensity was observed corresponding to the protonation of $LiNH_2$ to ammonia, which is enhanced during the deposition pulses, due to the increased proton availability related to HOR on the counter electrode.

As shown in Fig. 4A, LiF could be detected in all experiments, in which $LiBF_4$ was used, which is in accordance with previous studies showing that it is a crucial part of the SEI layer.[13,15,16,29,30] However, overall LiF signals were less pronounced compared to our previous work except for when 0.125 vol% water was added to the electrolyte. In all cases, LiF was detected at OCV prior to applying any current or potential, and often already in the first GI WAXS measurement. As electrolyte was only added after cell alignment, the presence of LiF in the first measurements indicates chemical $LiBF_4$ decomposition, which is then, over the course of the experiment, potentially aided by the X-ray beam.[31,32] DFT calculations suggest that the hydrolysis of $LiBF_4$ leads to the formation of LiF and HF, which could explain the comparatively strong LiF signals observed prior to Li plating when water had been added to the electrolyte (Fig. S10).[33] A lower proton concentration compared to previous experiments likely also plays a role in less pronounced LiF formation in experiments without water as HOR prevents electrolyte acidification due to electrolyte decomposition on the anode.[34] It has been proposed that diglyme can chelate the Li^+ ion in LiF increasing its solubility as a contact ion pair and inhibiting its aggregation which likely plays role in overall lower LiF intensities.[35,36] Chelation of Li^+ or even protons might further hinder LiF formation.

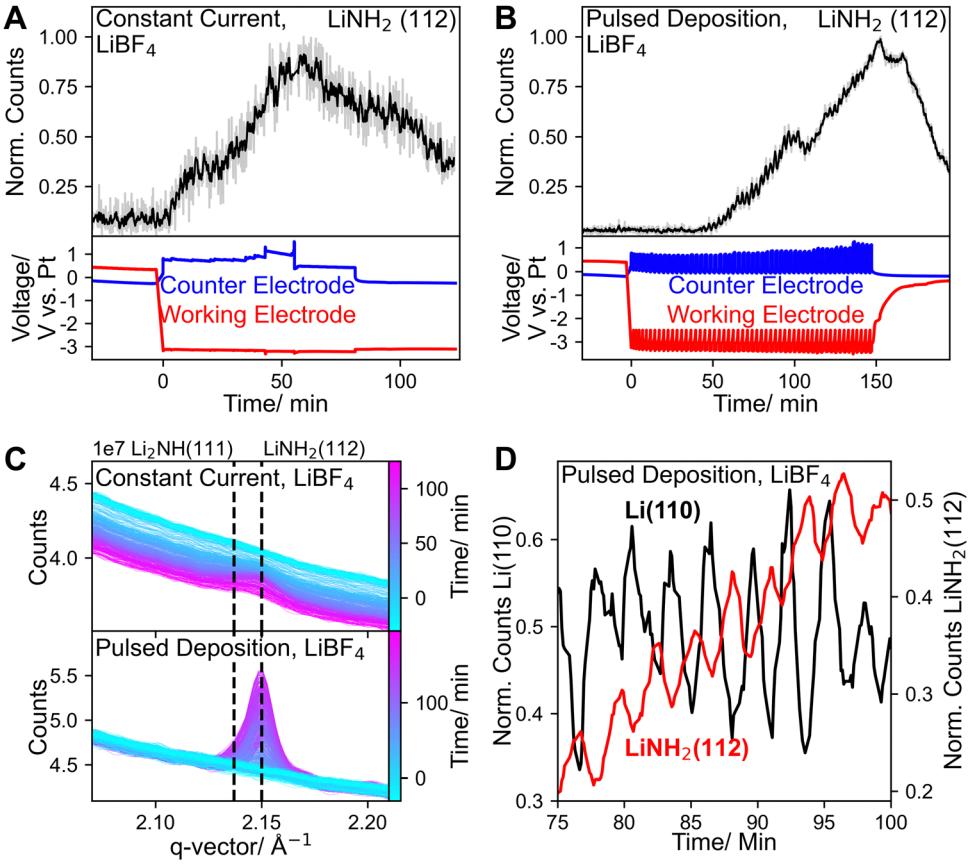

Fig. 3 Time traces of the $LiNH_2$ peak throughout constant current (A) and pulsed deposition (B) experiment. A linear background was subtracted from the integrated WAXS pattern, prior to determining peak maxima for the time traces. (C) Integrated WAXS patterns showing peaks attributed to the $LiNH_2$ (112) reflection. Diffractograms presented in cyan correspond to measurements earlier during the experiment, whereas diffractograms in magenta correspond to measurements later in the experiment. (D) Comparison of time traces corresponding to Li(110) and $LiNH_2$(112) for a pulsed deposition experiment. In constant current experiments a current of -4 mA cm^{-2} was applied until 7.5C was passed. In pulsed deposition experiments 54 cycles (corresponding to 5C) consisting of applying a current of -4 mA cm^{-2} for 1 min, followed by a resting period at OCV until the working electrode potential had increased to > -2.5 V *vs.* Pt were conducted. A Cu(111) single crystal was used as the working electrode and a Pt wire as reference electrode. A stainless-steel mesh with electrodeposited PtAu catalyst, supplied with H_2 was used as counter electrode. Electrolytes consisted of 1 M $LiBF_4$ dissolved in diglyme and 0.125 vol% EtOH.

In our previous work, an increase in LiF intensities was observed immediately upon applying an electrical potential. In contrast, here this immediate increase was not observed unless water had been added to the electrolyte (Fig. 4B). A high HF concentration in the electrolyte caused by the hydrolysis of $LiBF_4$ could explain increased LiF formation due to the reaction of HF with electrodeposited metallic Li. With added water both Li and LiF intensities increased throughout most of the experiment followed by a sharp decline after $\sim$50 min. This decrease coincided with an increase of the counter electrode potential, which was caused by bubble formation in the cell. This problem could be alleviated by temporarily increasing the electrolyte flow rate. It is unclear, however, whether the bubble or increased counter electrode potential were related to the decrease of Li and LiF signals. A rapid decrease in Li intensity could indicate accelerated reaction with the electrolyte, possibly caused by SEI cracking, leading to increased hydrogen and thereby bubble formation, which could lead to further SEI degradation. Lithium hydroxide, formed by the reaction of lithium and water, was also observed (Fig. S20). Without water, LiF intensity decreased during the experiment. While a low proton concentration and diglymes ability to form chelate complexes with Li^+ might explain suppressed LiF formation it cannot explain the apparent disappearance of LiF during Li plating. In our previous work, a decrease in LiF intensity accompanied by an increase in Li intensity was observed and attributed to Li plating beneath LiF, lifting it above the beam.[13] However, in this study, no increase in LiF intensity was observed when Li was no longer detectable, therefore the apparent disappearance of LiF cannot be explained by this mechanism. Another possibility is that flow of the electrolyte contributed to the physical removal of LiF from the electrode. Accordingly, after the experiments small amounts of visible deposits were found outside of the cell, however it seems unlikely that electrolyte flow alone could account for the complete disappearance of LiF peaks. As this change occurred only after current was drawn it is clear that the apparent disappearance of LiF is initiated by an electrochemical process during the experiment. As shown in Fig. 5A, in the experiments without

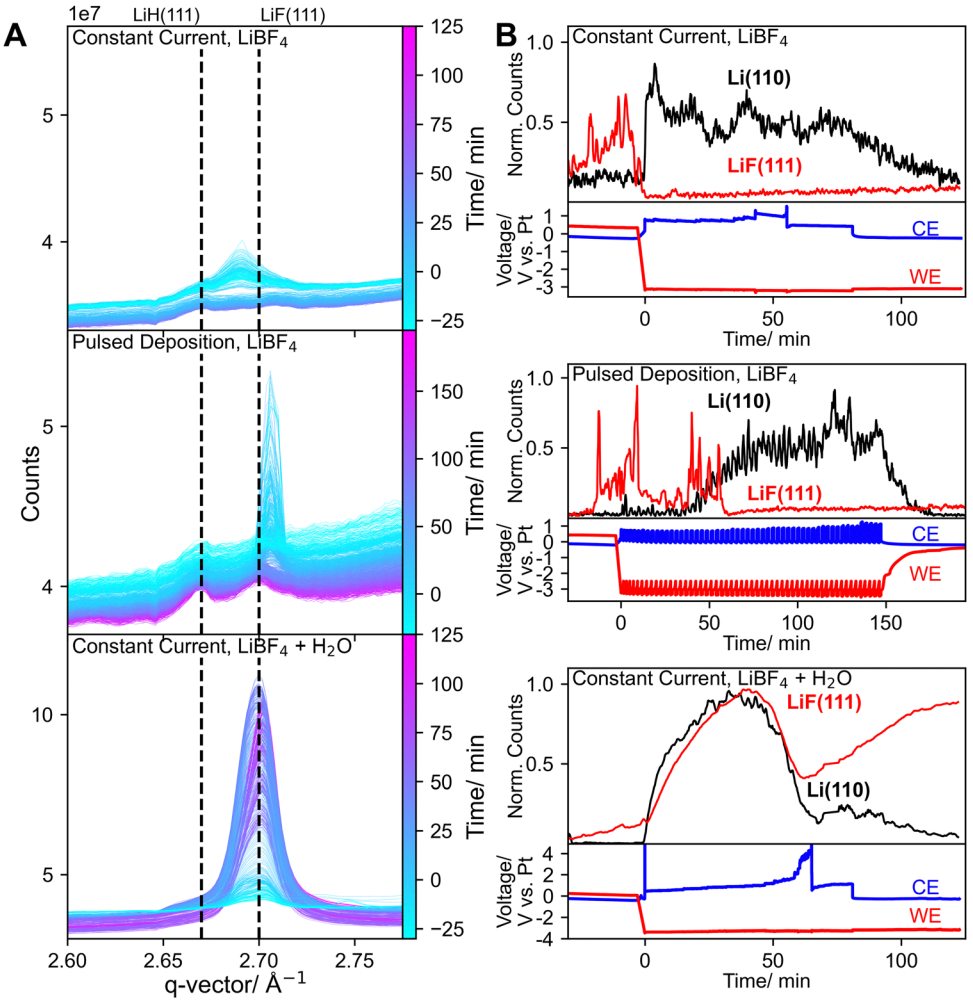

Fig. 4 (A) Integrated WAXS pattern showing the LiF(111) peak under different operating conditions. (B) Time traces of the LiF(111) peaks compared to that of the Li(110) peak under different operating conditions. In constant current experiments a current of -4 mA cm^{-2} was applied until 7.5C was passed. In pulsed deposition experiments 54 cycles (corresponding to 5C) consisting of applying a current of -4 mA cm^{-2} for 1 min, followed by a resting period at OCV until the working electrode potential had increased to > -2.5 V *vs.* Pt were conducted. A Cu(111) single crystal was used as the working electrode and a Pt wire as reference electrode. A stainless-steel mesh with electrodeposited PtAu catalyst, supplied with H_2 was used as counter electrode. Electrolytes consisted of 1 M $LiBF_4$ dissolved in diglyme and 0.125 vol% EtOH. In one experiment 1 vol% H_2O was added to the electrolyte.

water, peaks emerged, clearly showing the formation of a crystalline species, that we could not identify. These peaks were not observed in our previous study with THF-based electrolytes, indicating a significant difference in SEI composition and suggesting that the formation of these species is associated with diglyme.

As shown in Fig. 5B, the peaks corresponding to the unidentified species emerged in parallel to the disappearance of LiF peaks (Fig. 4B). This correlation indicates that either LiF is involved in their formation or they evolve under conditions that do not favor LiF formation. This is further supported by the observation that the unidentified species did not emerge when water had been added to the electrolyte and high LiF intensities were detected. Possibly a high proton concentration prevents the formation of these compounds, which could be related to the sharp drop in ammonia FE, previously reported at water concentrations above 17 mM.[17]

As shown in Fig. 5A more peaks were observed when pulsed deposition was used, compared to constant current deposition. In Fig. 5B the time development of the peaks with the highest intensities associated with the unidentified species in a pulsed deposition experiment are shown. All peaks emerge parallel to the decrease of LiF intensity, however there are two distinct sets of peaks, showing different time behaviors, indicating that there are two different species. As shown in Fig. 5A peaks only emerged at $q = 0.580$ Å^{-1} and $q = 0.834$ Å^{-1} implying only one of the species formed when -4 mA cm^{-2} constant current was used. Notably both species formed when -2 mA cm^{-2} constant current was used (Fig. S21), showing a possible relationship with electrochemical parameters. Possibly an electrochemical step is necessary for the formation of the observed compounds, or lower (effective) current densities promote crystallization. Another possibility is a dependence on electrolyte properties such as the proton concentration, which could explain the

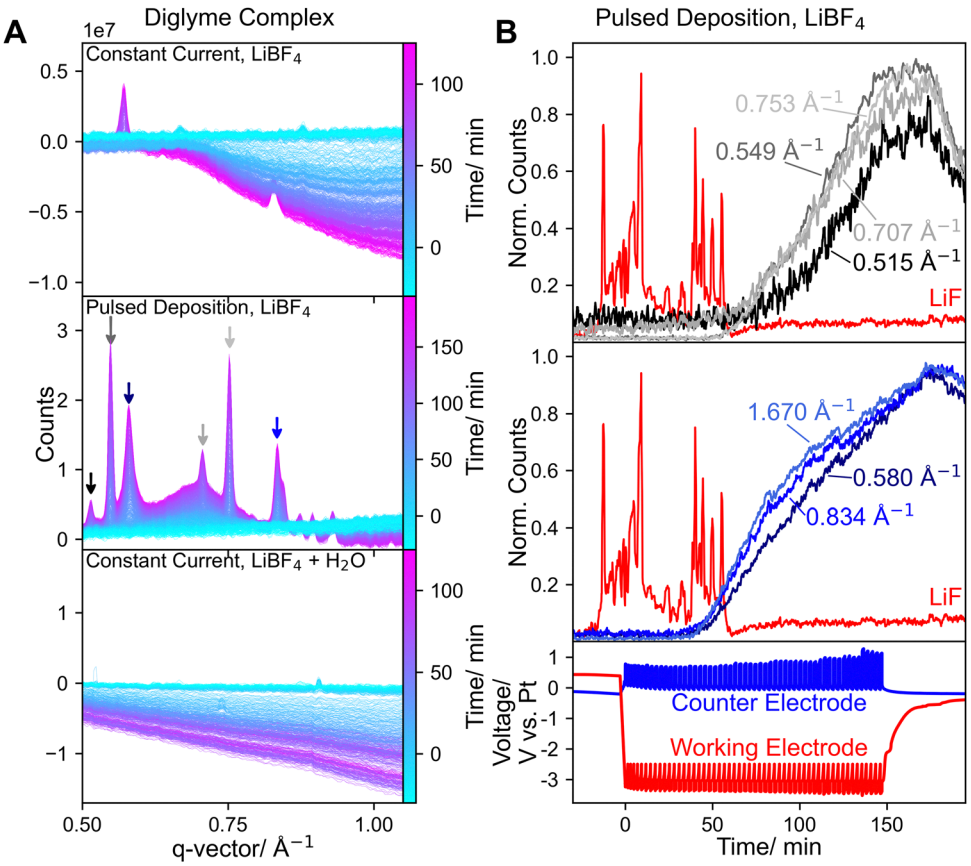

Fig. 5 (A) Integrated WAXS pattern showing peaks, possibly associated with a diglyme Li–salt complex under different operating conditions. The average of the first 5 frames, collected at OCV, was subtracted. (B) Time traces of the LiF(111) peak (red) and peaks associated with two unidentified diglyme complexes (blue or gray) observed when using pulsed deposition. The colors of the traces correspond to the peaks marked by arrows of the same color in (A). In constant current experiments a current of -4 mA cm^{-2} was applied until 7.5C was passed. In pulsed deposition experiments 54 cycles (corresponding to 5C) consisting of applying a current of -4 mA cm^{-2} for 1 min, followed by a resting period at OCV until the working electrode potential had increased to > -2.5 V *vs.* Pt were conducted. A Cu (111) single crystal was used as the working electrode and a Pt wire as reference electrode. A stainless-steel mesh with electrodeposited PtAu catalyst, supplied with H_2 was used as counter electrode. Electrolytes consisted of 1 M $LiBF_4$ dissolved in diglyme and 0.125 vol% EtOH. In one experiment 1 vol% H_2O was added to the electrolyte.

absence of both compounds in the presence of water. With a lower current density or pulsed deposition, in combination with electrolyte flow the proton concentration in the electrolyte in the cell is likely lower. It should be noted that in Fig. 5B a peak at q = 1.670 Å^{-1} was included (Fig. S22). This peak could also correspond to the Li_3N(001) reflection, however, due to the time development and the absence of other Li_3N peaks, the peak was attributed to the unidentified complex species. If small amounts of crystalline Li_3N were present during the experiment, corresponding signals might have overlapped with the described peak. More small peaks, likely associated mainly with the unidentified compounds were observed. However, it is possible that other species could not be identified if they were only present in small amounts.

Lithium ethoxide (LiEtO) has been shown to be part of the SEI layer in Li-NRR systems and its formation would depend on the proton concentration in the electrolyte (LiEtO + $H^+ \rightarrow Li^+ +$ EtOH).[37] Recorded reference spectra (Fig. S23) show that LiEtO has diffraction signals at similar but not the same q-vectors, observed in the experiments. It should be noted that different diffraction patterns were observed for a commercial sample and a sample synthesized from the reaction of Li with ethanol $\left(\mathrm{Li} + \mathrm{EtOH} \rightarrow \mathrm{LiEtO} + \frac{1}{2}\mathrm{H_2}\right)$. This suggests that multiple possible LiEtO crystal structures can form depending on reaction conditions, and that the unidentified peaks may be related to the formation of LiEtO.

Multiple crystalline complexes formed from different Li–salts and different glycol ethers have been previously reported as solid electrolytes for Li-batteries.[38–40] Given the low q-vectors at which the unidentified peaks were observed, it is plausible that comparable diglyme–Li–salt complexes, potentially serving as a solid electrolyte, were also formed during the presented experiments. Diglyme combined with $LiBF_4$ can form Li^+-conducting crystalline complexes in which the Li^+ ion of the electrolyte salt is coordinated by the diglyme ether groups. However, the diffraction patterns observed in the presented experiments differ from those previously reported for diglyme–$LiBF_4$ complexes.[38] The formation of a similar diglyme–LiF complex could explain the apparent absence of LiF in experiments

without water. While we were able to reproduce the synthesis of previously reported diglyme–$LiBF_4$ complexes (Fig. S24), we could not apply a similar synthesis to produce a corresponding diglyme–LiF compound. The synthesized diglyme–$LiBF_4$ complex was also successfully tested as a solid electrolyte (FE ≈ 10%; Fig. S25 and S26) and represents a starting point for the development of solid electrolytes for Li-NRR. It should also be noted that LiF was already detected before any current or potential was applied whereas the unidentified species were only detected afterwards. Therefore, diglyme, LiF, and $LiBF_4$ alone are not sufficient for their formation and an electrochemically initiated process is necessary. Lithium plating and the accompanying SEI formation lead to the formation of other species such as LiH, $LiNH_2$, or LiEtO that might be involved in the formation of the unidentified species. It is also possible that the electrochemically induced change is related to the solvent rather than the formation of a specific Li–salt. For example, the polymerization of diglyme could lead to the formation of longer-chained glymes. NMR analysis of diglyme-based electrolytes in long-term Li-NRR experiments, however, did not show significant changes in the solvent.[17]

Even though it was not possible to exactly determine the species giving rise to the diffraction patterns shown in Fig. 5A, it is reasonable to assume that they play a crucial role in the SEI layer. Given the low q-vectors at which the peaks appear and diglymes ability to form Li–salt complexes, it is a reasonable assumption that the unidentified species are crystalline diglyme complexes of one or multiple inorganic SEI species, such as LiF or LiEtO. Therefore, further research is necessary to identify and investigate the role of these species, especially considering the previously reported superior long-term stability of diglyme based electrolytes.[17] As shown in Fig. 5B, the intensity of all peaks increases continuously during the experiment and even for approx. 20 min at OCV. The continuing formation of any species, especially those not directly related to the formation of ammonia, is in general undesirable for long-term stability. However, after approx. 30 min at OCV a decrease in intensity was observed, possibly indicating the dissolution of the deposited complexes or that their formation is reversible. Understanding the exact role of these species is therefore critical in further improving Li-NRR performance and stability.

Lithium bis(trifluoromethanesulfonyl)imide (LiTFSI) and Lithium difluoro(oxalato)borate (LiFOB) have been reported as alternative electrolyte salts, that showed better performance than $LiBF_4$ in certain setups.[14,41,42] As shown in Fig. 6A, with both salts LiOH could be detected, which could indicate a higher water content in the salts. With LiTFSI both Li and $LiNH_2$ could clearly be detected, suggesting that an SEI layer had formed that could stabilize these compounds. However, aside from LiOH and LiH, no species could be detected indicating that the LiTFSI derived SEI mainly consists of non-crystalline species. Like in the $LiBF_4$ experiments no Li_3N could be observed, further confirming that $LiNH_2$ is the most stable, crystalline reaction intermediate towards ammonia formation. In the case of LiFOB, LiH and LiF were detected but no Li (or $LiNH_2$) could be observed, indicating that plated Li quickly reacted and dissolved. Given the comparatively low FE of only

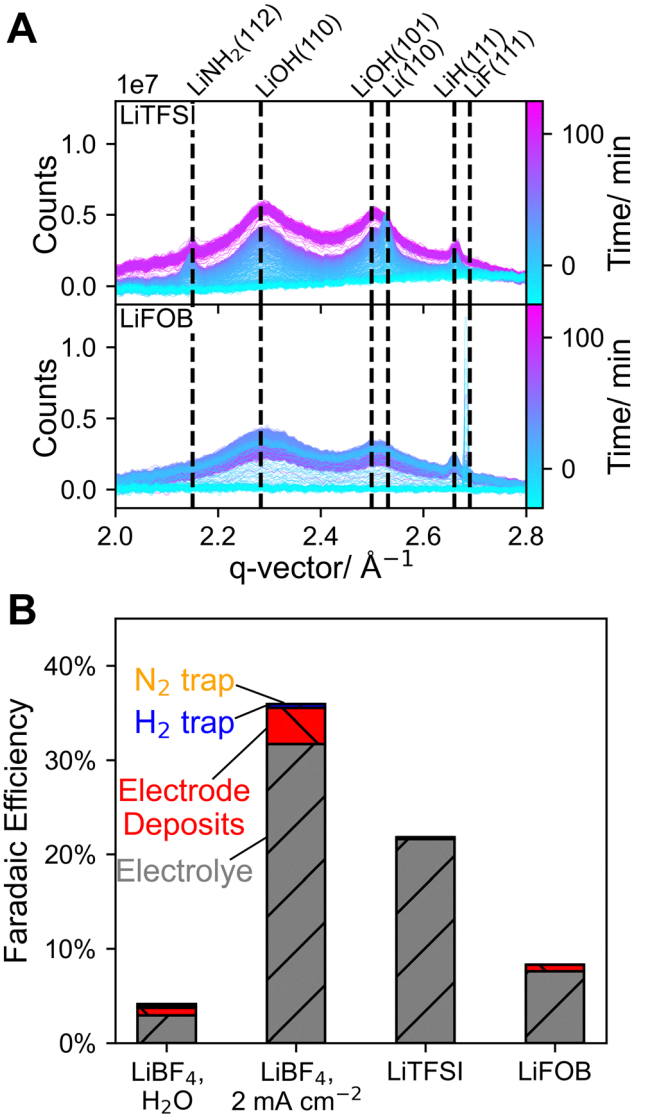

Fig. 6 (A) WAXS patterns showing different SEI species when using LiTFSI or LiFOB as electrolyte salt. The average of the first 5 frames, collected at OCV, was subtracted. (B) Ammonia faradaic efficiencies for different electrolyte compositions. In all experiments a current of −4 mA cm^{-2} was applied until 7.5C was passed. A Cu(111) single crystal was used as the working electrode and a Pt wire as reference electrode. A stainless-steel mesh with electrodeposited PtAu catalyst, supplied with H_2 was used as counter electrode. Electrolytes consisted of 1 M Li–salt ($LiBF_4$, LiTFSI or LiFOB) dissolved in diglyme and 0.125 vol% EtOH. In one experiment 1 vol% H_2O was added to the electrolyte.

8.2% (Fig. 6B), it is likely that most of the plated Li reacted with protons to form H_2, indicating that the formed SEI layer was not able to sufficiently limit proton transport to the plated Li. However, EtOH concentration was not optimized for either LiTFSI or LiFOB.

Notably, the diglyme complexes detected in $LiBF_4$ experiments could not be detected with LiTFSI or LiFOB suggesting that the electrolyte salt plays a critical role in its formation. Ionic association strength has been previously identified as a parameter influencing the stability of solid Li–salt complexes

with different glymes.[43] Of the here studied salts, $LiBF_4$ has the highest ionic association strength, which could explain why the unidentified complexes were only observed in $LiBF_4$ experiments.[44] As shown in Fig. 1B and 6B the highest FEs were achieved when the described complexes were detected, indicating their importance for Li-NRR performance. As mass transport characteristics play a large role in determining selectivity towards ammonia, it is reasonable to assume that these compounds have a beneficial effect on the diffusion of reactants through the SEI layer.[16,45] Nevertheless, more research is necessary to clearly determine the identity and properties of these unidentified species and the critical role of proton concentration in their formation.

Conclusion

GI WAXS was used to study the electrode deposits formed during Li-NRR under conditions that enabled record ammonia FEs for *in situ* and *operando* measurements. The improved setup enabled HOR on the anode, thereby eliminating the need for a sacrificial proton donor. These advances enabled an *operando* study under conditions close to state-of-the-art Li-NRR systems. The high FEs achieved provide direct insights into the Li-NRR mechanism with $LiNH_2$ clearly identified as the most stable crystalline reaction intermediate towards ammonia. Furthermore, it was shown that unlike in the $LiBF_4$/THF derived SEI, LiF is not a prominent component of the $LiBF_4$/diglyme SEI. Instead, two crystalline compounds, likely diglyme complexes, were observed as a crucial part of the SEI formed in the $LiBF_4$/diglyme system. While these compounds could not be definitively identified, their consistent presence suggests that they play a role in governing Li-NRR selectivity and stability. Their formation is also likely dependent on proton concentration, motivating further research in the exact role of protons in SEI formation. These findings highlight the importance of electrolyte composition and SEI chemistry in Li-NRR. Further research is needed to identify these SEI compounds and elucidate their properties, which will be critical for optimizing efficiency and long-term stability. Nevertheless, this study represents a starting point for the rational design of artificial SEI layers and solid electrolytes for Li-NRR.

Author contributions

Conceptualization: N. H. D., J. B. V. M., J. D., I. C. Data curation: N. H. D., J. B. V. M., V. A. N., J. B. P., V. V. Formal analysis: N. H. D., J. B. V. M., V. A. N., S. L., X. F. Investigation: N. H. D., J. B. V. M., V. A. N., J. B. P., V. V. Methodology: N. H. D., J. B. V. M., V. A. N., J. B. P, V. V, J. D. Software: N. H. D. Supervision: T. F. J., J. K., J. D., I. C. Writing – original draft: N. H. D. Writing – review & editing: N. H. D., J. B. V. M., V. A. N., J. B. P., V. V., S. L., X. F., T. F. J., J. K., J. D., I. C.

Conflicts of interest

There are no conflicts of interest to declare.

Data availability

Electrochemical data and overview diffractograms can be found in the supplementary information (SI). Supplementary information is available. See DOI: https://doi.org/10.1039/d5ee06529a.

GI WAXS data collected at the European Synchrotron Radiation Facility (ESRF) is available at https://doi.org/10.15151/ESRF-ES-1665529392.

Acknowledgements

We gratefully acknowledge the funding by Villum Fonden, part of the Villum Center for the Science of Sustainable Fuels and Chemicals (V-SUSTAIN II grant 54337). X. F. was supported under the MSCA European Postdoctoral Fellowships (Electro-Ammonia Project 101059643). V. A. N. was supported under the National Science Foundation Graduate Research Fellowship Program under grant no. DGE-1656518 and the Camille and Henry Dreyfus Foundation. We acknowledge the European Synchroton Radiation Facility (ESRF) for the provision of synchrotron radiation at beamline ID 31 (MA-6092; 10.15151/ESRF-ES-2003697977).

References

1 L. E. Apodaca, *Mineral commodity summaries 2023: NITROGEN (FIXED)—AMMONIA*, National Minerals Information Center, 2023.
2 International Energy Agency, Ammonia Technology Roadmap: Towards more sustainable nitrogen fertiliser production, OECD, 2021.
3 D. R. MacFarlane, P. V. Cherepanov, J. Choi, B. H. R. Suryanto, R. Y. Hodgetts, J. M. Bakker, F. M. Ferrero Vallana and A. N. Simonov, *Joule*, 2020, **4**, 1186–1205.
4 F. Haber and R. Le Rossignol, *Z. Elektrochem. Angew. Phys. Chem.*, 1913, **19**, 53–72.
5 S. Z. Andersen, V. Čolić, S. Yang, J. A. Schwalbe, A. C. Nielander, J. M. McEnaney, K. Enemark-Rasmussen, J. G. Baker, A. R. Singh, B. A. Rohr, M. J. Statt, S. J. Blair, S. Mezzavilla, J. Kibsgaard, P. C. K. Vesborg, M. Cargnello, S. F. Bent, T. F. Jaramillo, I. E. L. Stephens, J. K. Nørskov and I. Chorkendorff, *Nature*, 2019, **570**, 504–508.
6 J. Choi, B. H. R. Suryanto, D. Wang, H.-L. Du, R. Y. Hodgetts, F. M. Ferrero Vallana, D. R. MacFarlane and A. N. Simonov, *Nat. Commun.*, 2020, **11**, 5546.
7 A. Tsuneto, A. Kudo and T. Sakata, *Chem. Lett.*, 1993, 851–854.
8 A. Tsuneto, A. Kudo and T. Sakata, Lithium-mediated electrochemical reduction of high pressure N_2, to NH_3, *J. Electroanal. Chem.*, 1994, **367**, 183.
9 F. Fichter, P. Girard and H. Erlenmeyer, *Helv. Chim. Acta*, 1930, **13**, 1228–1236.
10 N. Lazouski, Z. J. Schiffer, K. Williams and K. Manthiram, *Joule*, 2019, **3**, 1127–1139.
11 S. J. Blair, M. Doucet, J. F. Browning, K. Stone, H. Wang, C. Halbert, J. Avilés Acosta, J. A. Zamora Zeledón,

A. C. Nielander, A. Gallo and T. F. Jaramillo, *ACS Energy Lett.*, 2022, **7**, 1939–1946.
12 S. J. Blair, M. Doucet, V. A. Niemann, K. H. Stone, M. E. Kreider, J. F. Browning, C. E. Halbert, H. Wang, P. Benedek, E. J. McShane, A. C. Nielander, A. Gallo and T. F. Jaramillo, *Energy Environ. Sci.*, 2023, **16**, 3391–3406.
13 N. H. Deissler, J. B. V. Mygind, K. Li, V. A. Niemann, P. Benedek, V. Vinci, S. Li, X. Fu, P. C. K. Vesborg, T. F. Jaramillo, J. Kibsgaard, J. Drnec and I. Chorkendorff, *Energy Environ. Sci.*, 2024, **17**, 3482–3492.
14 H.-L. Du, M. Chatti, R. Y. Hodgetts, P. V. Cherepanov, C. K. Nguyen, K. Matuszek, D. R. MacFarlane and A. N. Simonov, *Nature*, 2022, **609**, 722–727.
15 S. Li, Y. Zhou, K. Li, M. Saccoccio, R. Sažinas, S. Z. Andersen, J. B. Pedersen, X. Fu, V. Shadravan, D. Chakraborty, J. Kibsgaard, P. C. K. Vesborg, J. K. Nørskov and I. Chorkendorff, *Joule*, 2022, **6**, 2083–2101.
16 X. Fu, J. B. Pedersen, Y. Zhou, M. Saccoccio, S. Li, R. Sažinas, K. Li, S. Z. Andersen, A. Xu, N. H. Deissler, J. B. V. Mygind, C. Wei, J. Kibsgaard, P. C. K. Vesborg, J. K. Nørskov and I. Chorkendorff, *Science*, 2023, **379**, 707–712.
17 S. Li, Y. Zhou, X. Fu, J. B. Pedersen, M. Saccoccio, S. Z. Andersen, K. Enemark-Rasmussen, P. J. Kempen, C. D. Damsgaard, A. Xu, R. Sažinas, J. B. V. Mygind, N. H. Deissler, J. Kibsgaard, P. C. K. Vesborg, J. K. Nørskov and I. Chorkendorff, *Nature*, 2024, **629**, 92–97.
18 O. M. Magnussen, J. Drnec, C. Qiu, I. Martens, J. J. Huang, R. Chattot and A. Singer, *Chem. Rev.*, 2024, **124**, 629–721.
19 N. H. Deissler, V. Vinci, J. B. V. Mygind, X. Fu, S. Li, J. Kibsgaard, J. Drnec and I. Chorkendorff, *Next Energy*, 2025, **8**, 100279.
20 R. Feidenhans'l, *Surf. Sci. Rep.*, 1989, **10**, 105–188.
21 R. Haas, M. Murat, M. Weiss, J. Janek, A. Natan and D. Schröder, *J. Electrochem. Soc.*, 2021, **168**, 70504.
22 R. Sažinas, S. Z. Andersen, K. Li, M. Saccoccio, K. Krempl, J. B. Pedersen, J. Kibsgaard, P. C. K. Vesborg, D. Chakraborty and I. Chorkendorff, *RSC Adv.*, 2021, **11**, 31487–31498.
23 J. B. V. Mygind, N. H. Deissler, S. Li, X. Fu, J. Kibsgaard and I. Chorkendorff, *ACS Electrochem.*, 2025, **1**, 987–996.
24 S. Z. Andersen, M. J. Statt, V. J. Bukas, S. G. Shapel, J. B. Pedersen, K. Krempl, M. Saccoccio, D. Chakraborty, J. Kibsgaard, P. C. K. Vesborg, J. Nørskov and I. Chorkendorff, *Energy Environ. Sci.*, 2020, **13**, 4291–4300.
25 Y. Jiang and F. Ye, *Chem. – Eur. J.*, 2024, **30**, e202400424.
26 Q. Wang, B. Liu, Y. Shen, J. Wu, Z. Zhao, C. Zhong and W. Hu, *Adv. Sci.*, 2021, **8**, 2101111.
27 J. Bjarke Valbæk Mygind, J. B. Pedersen, K. Li, N. H. Deissler, M. Saccoccio, X. Fu, S. Li, R. Sažinas, S. Z. Andersen, K. Enemark-Rasmussen, P. C. K. Vesborg, J. Doganli-Kibsgaard and I. Chorkendorff, *ChemSusChem*, 2023, **16**, e202301011.
28 V. A. Niemann, M. Doucet, P. Benedek, N. H. Deissler, J. B. V. Mygind, S.-W. Lee, I. Rios Amador, W. Willoughby, I. Chorkendorff, A. Nielander, W. Tarpeh and T. Jaramillo, *J. Am. Chem. Soc.*, 2025, 12469–12480.
29 K. Steinberg, X. Yuan, C. K. Klein, N. Lazouski, M. Mecklenburg, K. Manthiram and Y. Li, *Nat. Energy*, 2022, **8**, 138–148.
30 M. He, R. Guo, G. M. Hobold, H. Gao and B. M. Gallant, *Proc. Natl. Acad. Sci. U. S. A.*, 2020, **117**, 73–79.
31 H. G. Steinrück, C. Cao, M. R. Lukatskaya, C. J. Takacs, G. Wan, D. G. Mackanic, Y. Tsao, J. Zhao, B. A. Helms, K. Xu, O. Borodin, J. F. Wishart and M. F. Toney, *Angew. Chem., Int. Ed.*, 2020, **59**, 23180–23187.
32 C. Cao, T. P. Pollard, O. Borodin, J. E. Mars, Y. Tsao, M. R. Lukatskaya, R. M. Kasse, M. A. Schroeder, K. Xu, M. F. Toney and H.-G. Steinrück, *Chem. Mater.*, 2021, **33**, 7315–7336.
33 S. Di Muzio, O. Palumbo, S. Brutti and A. Paolone, *J. Electrochem. Soc.*, 2022, **169**, 070523.
34 K. Krempl, J. B. Pedersen, J. Kibsgaard, P. C. K. Vesborg and I. Chorkendorff, *Electrochem. Commun.*, 2022, 4883–4891.
35 F. Chrétien, J. Jones, C. Damas, D. Lemordant, P. Willmann and M. Anouti, *J. Power Sources*, 2014, **248**, 969–977.
36 H. Gao, Y. Li, R. Guo and B. M. Gallant, *Adv. Energy Mater.*, 2019, **9**, 1900393.
37 E. J. McShane, V. A. Niemann, P. Benedek, X. Fu, A. C. Nielander, I. Chorkendorff, T. F. Jaramillo and M. Cargnello, *ACS Energy Lett.*, 2023, 4024–4032.
38 Y. G. Andreev, V. Seneviratne, M. Khan, W. A. Henderson, R. E. Frech and P. G. Bruce, *Chem. Mater.*, 2005, **17**, 767–772.
39 C. Zhang, Y. G. Andreev and P. G. Bruce, *Angew. Chem.*, 2007, **119**, 2906–2908.
40 P. G. Bruce and C. A. Vincent, *Faraday Trans.*, 1993, **89**, 3187.
41 R. Y. Hodgetts, H.-L. Du, T. D. Nguyen, D. MacFarlane and A. N. Simonov, *ACS Catal.*, 2022, 5231–5246.
42 A. Mangini, J. B. V. Mygind, S. G. Ballesteros, A. Pedico, M. Armandi, I. Chorkendorff and F. Bella, *Angew. Chem.*, 2025, e202416027.
43 W. A. Henderson, *J. Phys. Chem. B*, 2006, **110**, 13177–13183.
44 S.-D. Han, O. Borodin, J. L. Allen, D. M. Seo, D. W. McOwen, S.-H. Yun and W. A. Henderson, *J. Electrochem. Soc.*, 2013, **160**, A2100–A2110.
45 N. Lazouski, K. J. Steinberg, M. L. Gala, D. Krishnamurthy, V. Viswanathan and K. Manthiram, *ACS Catal.*, 2022, **12**, 5197–5208.